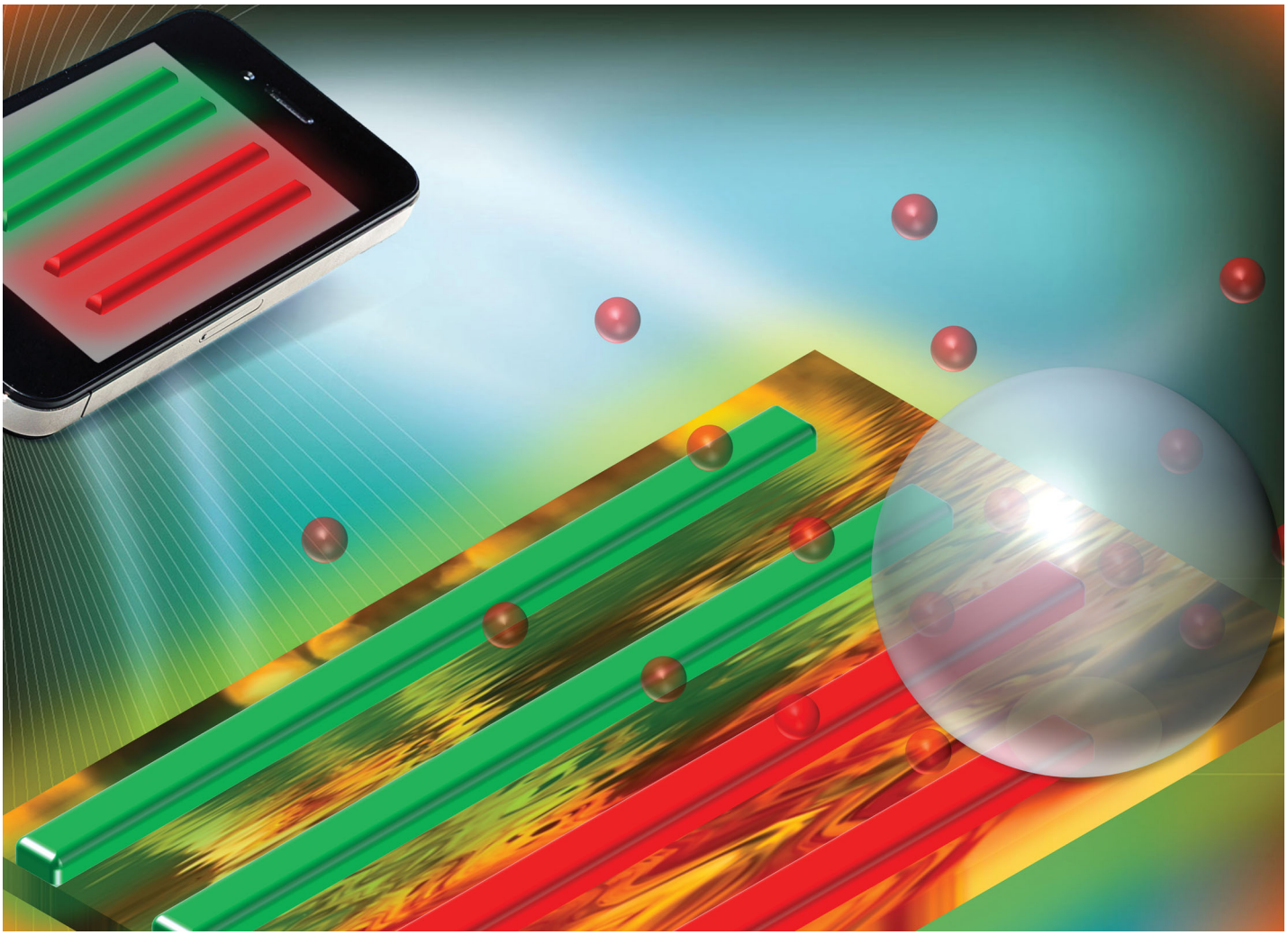

Showcasing a study on versatile patterning and fluorescence tuning of colloidal quantum dots *via* haptic-interfaced bubble printing by Prof. Yuebing Zheng's group at The University of Texas at Austin.

Patterning and fluorescence tuning of quantum dots with haptic-interfaced bubble printing

Translation of quantum dots (QDs) into many applications requires precise patterning of QDs with targeted properties on solid-state substrates. Haptic-interfaced bubble printing technique enables high-resolution (510 nm) high-throughput (>10^4 μm s^{-1}) patterning of QDs with a strong emission tunability.

As featured in:

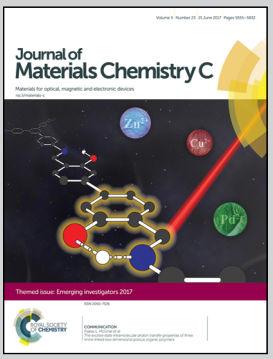

See Yuebing Zheng *et al.*, *J. Mater. Chem. C*, 2017, **5**, 5693.

ROYAL SOCIETY OF CHEMISTRY

rsc.li/materials-c

Registered charity number: 207890

Journal of Materials Chemistry C

PAPER

View Article Online
View Journal | View Issue

Cite this: J. Mater. Chem. C, 2017, 5, 5693

Patterning and fluorescence tuning of quantum dots with haptic-interfaced bubble printing†

Bharath Bangalore Rajeeva,[a] Majd A. Alabandi,[a] Linhan Lin,[a] Evan P. Perillo,[b] Andrew K. Dunn[b] and Yuebing Zheng *[a]

Received 26th January 2017,
Accepted 15th April 2017

DOI: 10.1039/c7tc00454k

rsc.li/materials-c

Semiconductor quantum dots (QDs) are attractive for a wide range of applications such as displays, light-emitting devices, and sensors due to their properties such as tunable fluorescence wavelength, high brightness, and narrow bandwidth. Most of the applications require precise patterning of QDs with targeted properties on solid-state substrates. Herein, we have developed a haptic-interfaced bubble printing (HIBP) technique to enable high-resolution (510 nm) high-throughput ($>10^4$ μm s^{-1}) patterning of QDs with strong emission tunability and to significantly enhance the accessibility of the technique *via* a smartphone device. The scalability and versatility of the HIBP are demonstrated in our arbitrary patterning of QDs on plasmonic substrates. A detailed study of plasmonic and photothermal interactions is performed *via* programmed stage movements to realize tunability of the emission wavelength and lifetime. Finally, the influence of the hand movement on the properties of the printed QDs in terms of emission wavelength tuning from yellow to blue is established. This work provides a single-step macroscale platform to manipulate nanoscale properties at high resolution and high throughput.

Introduction

Colloidal semiconductor quantum dots (QDs) have shown tremendous scientific and technological impact. For example, QDs exhibit exceptional optoelectronic properties due to their size-dependent quantum confinement effect, which enables tunable light emission with narrow bandwidth and high brightness.[1–3] One can further enhance the optical performances of QDs by positioning them in the proximity of plasmonic substrates, leading to improved emission rates and directionality.[4] In addition, the development of bulk solution-phase synthesis of QDs in both aqueous and non-aqueous solvents has significantly enhanced their applicability.[5–7] So far, QDs have been explored for various applications such as light-emitting devices,[8] displays,[9] photovoltaics,[10] biosensing,[11] lasers,[12] and photodetectors.[13]

The applications can be greatly improved by the capability of fabricating spatially addressable patterns of QDs with precisely tuned properties.[14,15] Chen *et al.* achieved laser-induced tunability of optical properties of self-assembled films of QDs.[16] However, with the self-assembly process, it is challenging to achieve site-specific deposition of QDs on the substrates. Due to their simplicity, additive nature, and real-time configurability *via* digital control,[17] direct-write techniques such as inkjet printing, electrohydrodynamic jet printing, and gravure printing have been explored to realize the site-specific deposition of QDs with high throughput and material saving. However, these traditional printing techniques have their resolution limited at the micrometer scale due to technological issues such as ink coalescence and oversizing.[18] In addition, tedious multi-step synthesis and deposition are needed to pattern QDs of variable optical properties on the same substrates, as required for some of the applications.[19] Hence, the development of a widely accessible printing technique with sub-micrometer resolution and fluorescence-tuning capability is highly desired to expand the applications of QDs.

In this work, we have developed and applied a haptic-interfaced bubble printing (HIBP) technique for free-form patterning and fluorescence tuning of QDs on plasmonic substrates. Bubble printing exploits the photothermal heating of the substrates to generate bubbles, which capture and immobilize the QDs at the substrate–solution interfaces *via* coordinated actions of Marangoni convection, surface tension, van der Waals interaction, and thermal adhesion.[20] The integration of a haptic interface into printing techniques caters to the engineering demands for precise and interactive processes at the micro- and nanoscale.[21] In our case, we integrate the printing process with a smartphone to achieve the haptic operation. Specifically, we have applied HIBP to achieve site-specific patterning of QDs on plasmonic substrates consisting of Au nanoislands (AuNI). The effects of printing

[a] *Materials Science and Engineering Program, Department of Mechanical Engineering, The University of Texas at Austin, Austin, Texas 78712, USA. E-mail: zheng@austin.utexas.edu*
[b] *Department of Biomedical Engineering, The University of Texas at Austin, Austin, Texas 78712, USA*

† Electronic supplementary information (ESI) available. See DOI: 10.1039/c7tc00454k

conditions on the emission characteristics of the patterned QDs in terms of emission wavelength and lifetime are studied based on both programmed stage control and haptic operation. By optimizing the printing parameters, we demonstrate simultaneous high resolution (510 nm linewidth) and high throughput ($>10^4$ μm s^{-1}) HIBP, with the QD emission wavelengths tuned across the visible spectrum. The haptic integration provides a single-step macroscale platform to manipulate properties at the nanoscale.

Experimental

Quantum dot synthesis

The water-soluble CdSe/CdS core/shell QDs with red (615 nm) and yellow (565 nm) emission were synthesized based on a recently reported method (Fig. 1a).[22] The synthesized QDs were purified and stored in chloroform. The QD concentrations were determined using the extinction coefficients.[23,24] An amphiphilic polymer (PMAO-PEG) (molar ratio of PMAO : PEG was 1 : 10) was obtained from the overnight reaction of poly(maleic anhydride-*alt*-1-octadecene) (PMAO, M_n = 30 000–50 000, Aldrich) and amino poly(ethylene glycol) methyl ether (mPEG-NH_2, MW 6000) in chloroform. The QDs and PMAO-PEG were mixed and stirred in chloroform for one hour at room temperature (molar ratio of QD : PMAO-PEG was 1 : 10). An equal amount of water and chloroform was added, and chloroform was gradually removed *via* rotary evaporation at room temperature, leading to clear and colored solution of water-soluble QDs. An ultracentrifuge (Beckman Coulter Optima L-80XP) was used to further concentrate and remove excess amphiphilic polymer.

Bubble printing and haptic interfacing

The printing was performed by programmed translation of a plasmonic substrate located on an automated optical stage. To prepare the plasmonic substrate, a 4 nm Au thin film was deposited on a glass substrate using thermal deposition (Denton Thermal evaporator), and the sample was subsequently annealed at 550 °C for 2 hours. The printing process was achieved using a Prior Proscan scientific stage (x–y resolution = 14 nm) in conjunction with a motorized flipper (ThorLabs MFF102, 500 ms response time) that performed the function of a shutter. A custom-written LabView code guided the stage along the predetermined coordinates and an on/off shutter status.

To achieve haptic operation, an android app registered the coordinates and the shutter status, which were subsequently imported into the LabView code. The mobile app was built on the Android Studio platform using Java, and it is compatible with all Android OS phones and tablets.

Characterization techniques

The fluorescence images were obtained using a Zeiss LSM 710 microscope with a 405 nm excitation source. All patterned samples were washed with DI water and dried with nitrogen gas before we performed the characterization. The composite images without any emission filters were generated *via* the wavelength-integrated coloring feature in the Zeiss ZEN software, thereby depicting the actual emission color of the printed QDs. The fluorescence lifetime of the QDs was measured *via* time-correlated single photon counting (TCSPC), using a femtosecond titanium:sapphire laser tuned to 800 nm (~200 fs) (Mira 900, Coherent), galvo scanning mirrors (6215H, Cambridge Tech.), and a GaAsP photomultiplier tube (PMT) (H7422PA-40, Hamamatsu) in a nondescanned detection scheme. The output current of the PMT was amplified using a preamplifier with 2 GHz cutoff (HFAC-26, Becker and Hickl GmbH). The amplified pulses from the PMTs were sent to the TCSPC module (SPC-150, Becker and Hickl GmbH). A silicone oil-immersion lens with NA of 1.3 (UPLSAPO60X, Olympus) was used. The fluorescence lifetime was recorded with a 20 ps time resolution, a pixel integration time of 5 ms and an incident

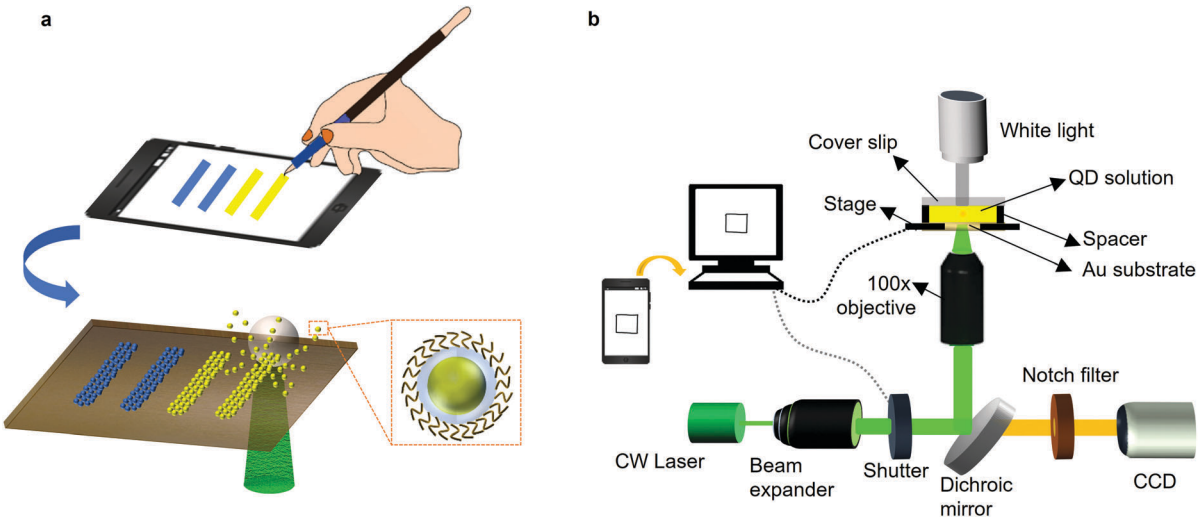

Fig. 1 Haptic-interfaced bubble printing: (a) Illustration of haptic-interfaced bubble printing (HIBP). QDs in a single aqueous suspension can be immobilized on the substrate to exhibit variable emission wavelengths based on the hand movement over the smartphone screen, which in turn is replicated in the printing process. The bottom inset shows a magnified view of the CdSe/CdS QD along with an amphiphilic coating of PMAO-PEG. (b) Schematic representation of the experimental setup for the haptic-interfaced bubble printing.

power of 1 mW. A least-squares method using the model of a single exponential decay convolved with a Gaussian impulse function was utilized to perform lifetime fitting. High fitting quality was ensured by removing data points with less than 500 photons, and the fittings with χ^2 values less than 2 were discarded. Atomic force microscopy (AFM) images were taken using a Park Scientific AFM under non-contact mode.

Results and discussion

Fig. 1a illustrates that HIBP can utilize a single QD solution to pattern QDs with variable emission characteristics on the plasmonic substrate. A laser beam focused with a 100× oil objective is used to print the QDs over a plasmonic substrate, which is positioned on an automated stage (Fig. 1b). The capture and immobilization of the QDs benefit from the plasmon-enhanced photothermal response of the AuNI substrate.[20,25] Briefly, upon incidence of a continuous wave laser beam (532 nm) on the AuNI substrate, the reemitted energy from the resonant AuNI *via* non-radiative Landau damping leads to overheating of water molecules to generate mesobubbles over the substrate surface. The Marangoni convection arising from the temperature gradient creates a convective drag force towards the bubble surface. The QDs are subsequently trapped *via* multi-force balance of vapor–liquid pressure difference, drag force and surface tension, and eventually immobilized on the substrate due to van der Waals interaction and thermal adhesion.

The large-area printing of QDs becomes feasible due to the high stability and low equilibration time ($\sim 10^{-4}$ s) of the sub-micron bubble[26] and the uniform temperature increase over the AuNI substrate.[27] The printing of arbitrary patterns of QDs is achieved through computer-controlled translation of the automated optical stage that holds the substrate. The printing is switched on and off using a motorized shutter, which reduces the incident laser power below the threshold power in the off state and results in bubble dissolution.

To enable the haptic operation of the bubble printing, we utilize a smartphone app and define the desired hand-drawn patterns over the display. The app presents a plain drawing space, a colored pallet, as well as buttons to save, erase/undo, and start a new pattern (Fig. S1, ESI†). We utilize Android's built-in coordinate system to register the haptic pattern and touch event to populate the vector coordinate and shutter matrix (Fig. S2 and Video S1, ESI†). The app-registered data are transferred to the custom-written LabView code to direct the printing process.

As an example, an inward spiral pattern of red QDs (Fig. 2a) was fabricated by the HIBP. The printed spiral has an overall dimension of ~30 μm and sub-micron linewidth. We can further perform scaling when translating the pattern from the smartphone coordinate system based on its resolution (2560 × 1440) to the actual print coordinates (in μm). The sub-micron resolution of HIBP enables us to control the dimensions of the printed QDs over a large range from a few micrometers to tens of micrometers. Based on the shapes hand-drawn over the smartphone (Fig. 2b) and the scaling factors ranging from 20× to 40×, we replicate the patterns of red QDs with different dimensions from 35 μm × 12 μm to 68 μm × 25 μm. Higher downscaling factors lead to smaller dimensions. The scalability of the pattern dimensions is useful for many applications such as multi-sensor integration with each sensor fabricated at a different dimension for enhanced performance.[28] The bright-field images of the QD patterns in Fig. 2 are shown in Fig. S3 (ESI†).

To provide guidance on fluorescence tuning of QDs in HIBP, we have shown that the bubble-printing process and the properties of the resulting QD patterns primarily depend on the interplay of three parameters: (i) stage translation speed, (ii) stage hold time, and (iii) line spacing in the patterns. We have systematically studied the influence of stage translation speed and line spacing on the fluorescence properties of yellow QDs patterned on the plasmonic substrate. As shown in Fig. 3a, three patterns consisting of parallel lines with gradually decreasing line spacing from 4 μm to 0.5 μm were fabricated at stage speeds of 1 μm s^{-1}, 6 μm s^{-1} and 10^4 μm s^{-1} (the highest speed), respectively. The printed QDs can achieve sub-micron linewidths down to 510 nm (Fig. S4, ESI†). From the fluorescence

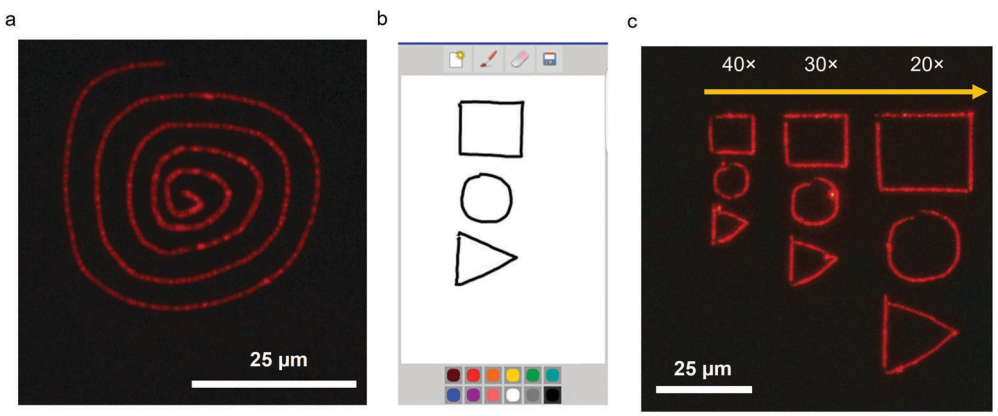

Fig. 2 Haptic printing and pattern scalability: (a) a hand-drawn spiral pattern over the smartphone is printed using red QDs on a plasmonic substrate. The fluorescence image of the spiral under the tetramethylrhodamine (TRITC) channel is shown. (b) A snapshot of the basic shapes drawn on the smartphone screen. (c) HIBP of the pattern in (b) using red QDs at different downscaling factors.

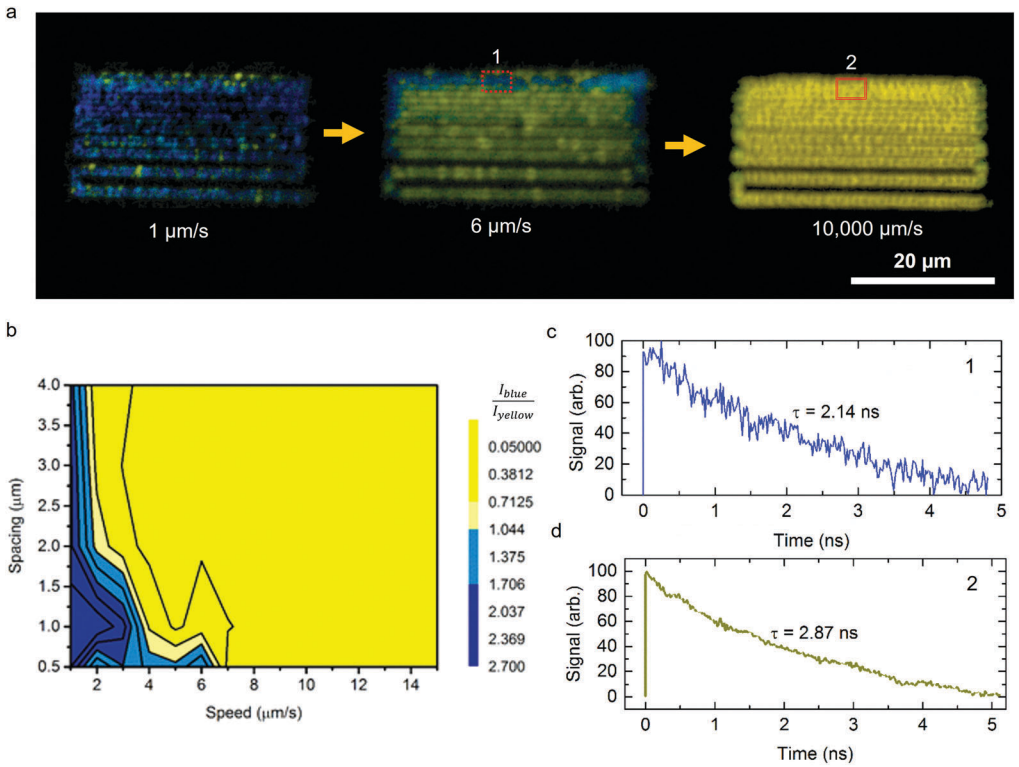

Fig. 3 Effects of stage speed and line spacing on the emission characteristics of the printed QDs on the plasmonic substrates: (a) Merged fluorescence images of patterns of yellow QDs printed with various stage speeds and line spacing. For each pattern, the line spacing decreases from 4 μm to 0.5 μm (from bottom to top). The blue shifts occur at lower stage speeds and smaller line spacing. (b) A contour plot of the ratio of the peak intensities for the blue (450–495 nm) and yellow (560–595 nm) light as a function of stage speed and line spacing. (c and d) Fluorescence lifetime of the printed QD at the region marked as 1 and 2 in (a). The lifetime decreases at smaller line spacing and slower stage speeds.

images in Fig. 3a, we can see that the emission of QDs makes a shift from the original yellow to blue color with decreasing stage speed and line spacing. The QDs printed with the lowest stage speed (1 μm s^{-1}) exhibit blue emission irrespective of the line space. At an intermediate stage speed of 6 μm s^{-1}, the effect of line spacing on the fluorescence wavelength is evident, with blue emission occurring at the lowest space of 0.5 μm.

We attribute the spectral shifts to the oxidation of QDs during the bubble printing. Due to the resonant heating upon laser irradiation, the temperature at the plasmonic nanoparticle surfaces can reach >100 °C.[20] Such elevated temperatures can lead to photo-oxidation of the printed QDs, which reduces the effective size of the QDs and thus causes a spectral blue-shift.[29,30] The rapid photo-oxidation process can limit the introduction of multiple non-radiative states on the QD surfaces, minimizing the influence on the quantum yield and brightness of the QDs.[29] The bubble printing at the lowest stage speed (1 μm s^{-1}) has the maximum laser-heating effect and the photo-oxidation is sufficient to have the QDs emit blue light irrespective of the line space. For the bubble printing at an intermediate stage speed of 6 μm s^{-1}, the blue emission occurs at the lowest space of 0.5 μm because the increased laser exposure from double scanning increases the photo-oxidation of the QDs. With higher stage speeds, the exposure time of the printed QDs to the laser heating isn't long enough to cause significant photo-oxidation (Video S2, ESI†). Fig. 3b shows a contour plot of the ratio of the peak intensities for blue (450–495 nm) and yellow (560–595 nm) light as a function of stage speed and line spacing. We can see that fine-tuning of the emission color of the printed QDs is possible by controlling the stage speed and line spacing.

We have further characterized the spontaneous emission rate of the printed QDs on plasmonic substrates by time-resolved fluorescence spectroscopy. As shown in Fig. 3c and d, the printing of QDs with a low speed resulted in a shorter lifetime (τ = 2.14 ns) compared to the ultra-fast printing (τ = 2.87 ns). The reduction in lifetime is attributed to the decrease in QD size in the low-speed printing, which has been reported previously.[31,32] In the smaller QD, a higher degree of overlap between the electron and hole wave functions leads to faster electron–hole recombination and thus a shorter lifetime.[33]

The reduction in the radiative lifetime from τ = 7.50 ns for QDs drop-cast on glass substrates (Fig. S5a, ESI†) to $\tau \approx$ 2.14 ns for the printed QDs (Fig. 3c) can be attributed to a combination of the oxidation of QDs and Purcell effect originating from the plasmonic substrate's proximity to the QDs.[34] The high-speed HIBP-printed QDs (τ = 2.87 ns) had a comparable lifetime to QDs drop-cast on AuNI ($\tau \approx$ 3.20 ns) (Fig. S5b, ESI†), with the additional reduction arising from the strong adhesion of QDs and thus the shorter QD–AuNI separation. The strong adhesion of the QDs to the substrate is further demonstrated by the consistency of the fluorescence images before and after sonication of the sample in DI water for 5 min (Fig. S6, ESI†). We further

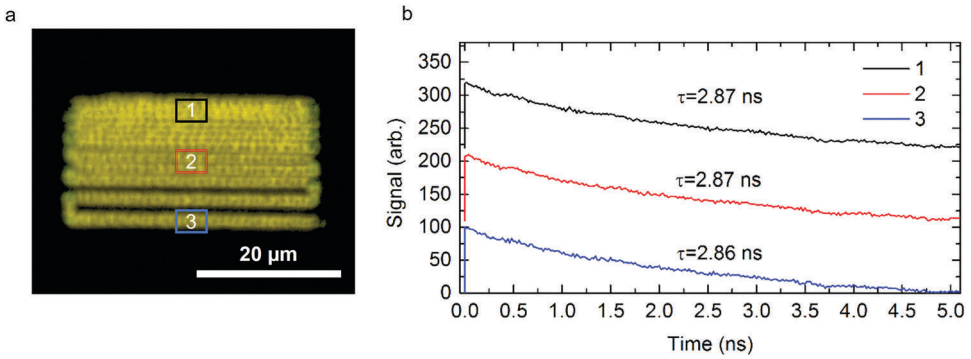

Fig. 4 Fluorescence lifetime measurements at various regions (with different line spacing) of the patterned QDs on the plasmonic substrate by ultra-fast bubble printing. (a) Fluorescence image of the QD pattern printed at an ultra-high speed of 10^4 μm s^{-1}. (b) Fluorescence lifetime of the QDs at the regions marked by 1, 2 and 3 in (a), with a *y*-offset.

performed the lifetime measurements at various regions (with different line spacing) of the QD pattern by ultra-fast bubble printing (Fig. 4). We can see that there is a negligible change (standard deviation $\approx$ 0.01 ns) in the lifetime at various line spacing. In this case, the photo-oxidation of the QDs is minimal and the increase in the spontaneous emission rate is primarily due to the Purcell effect. The lifetime tuning of the QDs in the bubble printing can be utilized to encode optical security devices and to study biological processes.[35]

Following the establishment of the process–structure–property relationship for the patterned QDs by bubble printing, we move on to demonstrate the fluorescence tuning of the printed QDs with the haptic operation. The density of coordinates in the coordinate matrix input into the LabView program is based on the speed of the hand movement over the smartphone display. Fig. 5a shows that the coordinate density is increased from 0.2 coordinate per μm to 10 coordinates per μm when the speed of the hand movement is decreased. The increase in the coordinate density is manifested as a decrease in the printing speed since the stage has an inherent hold time at each coordinate. Therefore, blue emission is observed from the QDs patterned at a coordinate density of >7 coordinates per μm, which leads to an effective stage speed of <3 μm s^{-1} (Fig. 5b). This observation is consistent with the contour plot in Fig. 3b. Fig. 5c shows the corresponding

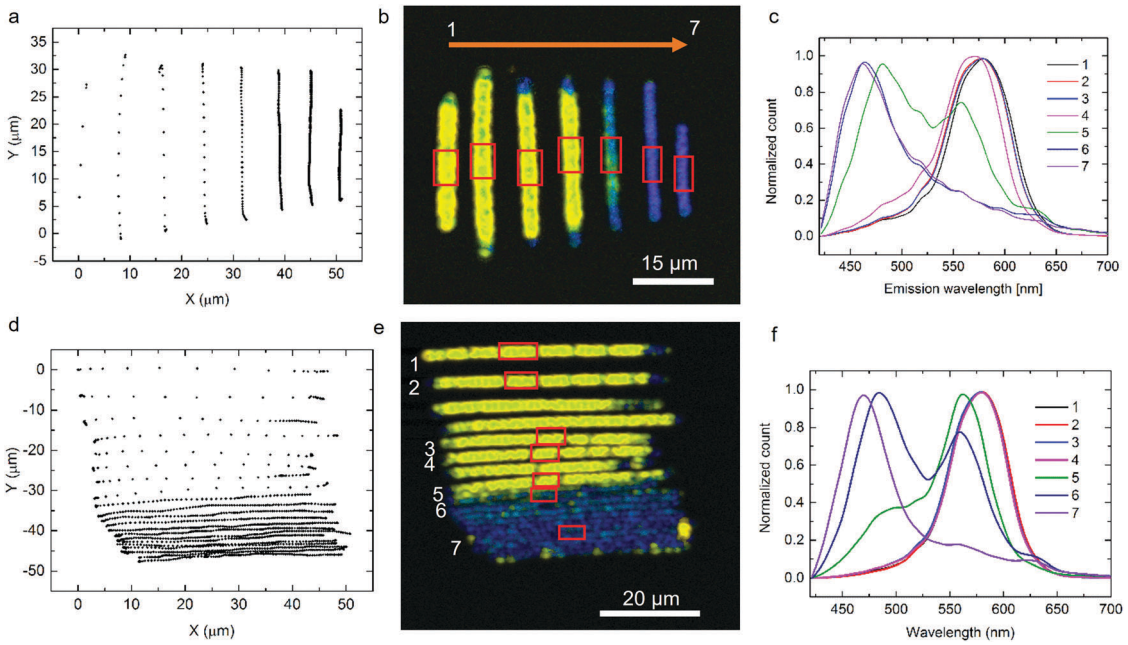

Fig. 5 Fluorescence tuning of the patterned QDs on plasmonic substrates by HIBP: (a) the registered coordinates from the smartphone based on hand-drawn lines with decreasing hand movement speed (from left to right). (b) Fluorescence image of the corresponding patterns of yellow QDs by HIBP based on the hand-drawn lines in (a). Blue emission occurs from the printed QDs at the slower hand movement. (c) Fluorescence spectra of the corresponding marked regions on the lines of QDs in (b). (d) The registered coordinates from the smartphone based on hand-drawn patterns combining the variations of hand movement speed and line spacing. (e) Fluorescence image of the corresponding patterns of yellow QDs by HIBP based on the hand-drawn lines in (d). (f) Fluorescence spectra recorded from the marked regions in (e). The rectangles in (b) and (e) indicate the regions from which the fluorescence spectra are recorded. The numbers in (b) and (e) correspond to those in (c) and (f), respectively.

fluorescence spectra for the lines of QDs in Fig. 5b. There is initially a minimal blue shift in the peak wavelength, followed by prominent blue shift for the three slowest hand-written lines. In addition, the spectrum broadens at the slower hand movement due to the continued photo-oxidation.[30]

We further combine hand movement speed with line spacing in the hand-drawn patterns to tune the QD fluorescence. Fig. 5d shows the coordinates with a simultaneous decrease in the hand movement speed and line spacing upon moving away from the origin along the *y*-axis. From the fluorescence image in Fig. 5e, we can see that blue emission starts to appear at the slower movement speed. With the reduced line spacing that leads to double exposure of the QDs to the laser beam, the blue emission is observed at a relatively low coordinate density of 4 coordinates per μm (compared to >7 coordinates per μm in Fig. 5b). The blue shift is also evidenced from the fluorescence spectra (Fig. 5f) taken at various locations in the QD pattern. Thus, we can pattern the QDs and tune their site-specific emission properties at the sub-microscale level by simply controlling hand movement over the smartphone display.

Conclusion

We have developed and applied HIBP to achieve versatile patterning of QDs on plasmonic substrates. An android app was utilized as a platform to register haptic movements as coordinates and to direct the printing process in a free form. HIBP has achieved a high printing speed ($>10^4$ μm s^{-1}), high resolution ($\sim$510 nm) and high pattern scalability, as well as the ability to simultaneously tune the fluorescence properties of the printed QDs. The tuning of fluorescence wavelength and lifetime of the QDs is achieved by controlling the plasmonic and photothermal effects in the HIBP. HIBP is readily applied to pattern other types of colloidal particles. By providing a highly accessible tool to manipulate matter at the nanoscale, HIBP can significantly advance research and education in nanoscience and nanotechnology.

Acknowledgements

The authors acknowledge the financial support of the Beckman Young Investigator Program, and Dr William W. Yu for providing the quantum dots. We also thank Mr Xiaolei Peng, Ms Ashwini Venkatesh, and Ms Priyanka Khante for helpful discussions.

References

1 X. Q. Li, Y. W. Wu, D. Steel, D. Gammon, T. H. Stievater, D. S. Katzer, D. Park, C. Piermarocchi and L. J. Sham, *Science*, 2003, **301**, 809–811.
2 D. Vanmaekelbergh and P. Liljeroth, *Chem. Soc. Rev.*, 2005, **34**, 299–312.
3 J. Y. Kim, O. Voznyy, D. Zhitomirsky and E. H. Sargent, *Adv. Mater.*, 2013, **25**, 4986–5010.
4 J. M. Pietryga, Y. S. Park, J. H. Lim, A. F. Fidler, W. K. Bae, S. Brovelli and V. I. Klimov, *Chem. Rev.*, 2016, **116**, 10513–10622.
5 Y. D. Yin and D. Talapin, *Chem. Soc. Rev.*, 2013, **42**, 2484–2487.
6 W. W. Yu and X. G. Peng, *Angew. Chem., Int. Ed.*, 2002, **41**, 2368–2371.
7 E. Cassette, M. Helle, L. Bezdetnaya, F. Marchal, B. Dubertret and T. Pons, *Adv. Drug Delivery Rev.*, 2013, **65**, 719–731.
8 B. S. Mashford, M. Stevenson, Z. Popovic, C. Hamilton, Z. Q. Zhou, C. Breen, J. Steckel, V. Bulovic, M. Bawendi, S. Coe-Sullivan and P. T. Kazlas, *Nat. Photonics*, 2013, **7**, 407–412.
9 T. H. Kim, K. S. Cho, E. K. Lee, S. J. Lee, J. Chae, J. W. Kim, D. H. Kim, J. Y. Kwon, G. Amaratunga, S. Y. Lee, B. L. Choi, Y. Kuk, J. M. Kim and K. Kim, *Nat. Photonics*, 2011, **5**, 176–182.
10 X. Z. Lan, S. Masala and E. H. Sargent, *Nat. Mater.*, 2014, **13**, 233–240.
11 I. L. Medintz, A. R. Clapp, H. Mattoussi, E. R. Goldman, B. Fisher and J. M. Mauro, *Nat. Mater.*, 2003, **2**, 630–638.
12 A. D. Lee, Q. Jiang, M. C. Tang, Y. Y. Zhang, A. J. Seeds and H. Y. Liu, *IEEE J. Sel. Top. Quantum Electron.*, 2013, **19**, 1901107.
13 G. Konstantatos, I. Howard, A. Fischer, S. Hoogland, J. Clifford, E. Klem, L. Levina and E. H. Sargent, *Nature*, 2006, **442**, 180–183.
14 K. E. Sapsford, T. Pons, I. L. Medintz and H. Mattoussi, *Sensors*, 2006, **6**, 925–953.
15 L. Zhang, C. Chen, W. J. Li, G. H. Gao, P. Gong and L. T. Cai, *ACS Appl. Mater. Interfaces*, 2016, **8**, 13187–13191.
16 J. X. Chen, Y. H. Chan, T. L. Yang, S. E. Wark, D. H. Son and J. D. Batteas, *J. Am. Chem. Soc.*, 2009, **131**, 18204–18205.
17 M. Singh, H. M. Haverinen, P. Dhagat and G. E. Jabbour, *Adv. Mater.*, 2010, **22**, 673–685.
18 J. R. Castrejon-Pita, W. R. S. Baxter, J. Morgan, S. Temple, G. D. Martin and I. M. Hutchings, *Atomization Sprays*, 2013, **23**, 541–565.
19 I. L. Medintz, H. T. Uyeda, E. R. Goldman and H. Mattoussi, *Nat. Mater.*, 2005, **4**, 435–446.
20 L. H. Lin, X. L. Peng, Z. M. Mao, W. Li, M. N. Yogeesh, B. B. Rajeeva, E. P. Perillo, A. K. Dunn, D. Akinwande and Y. B. Zheng, *Nano Lett.*, 2016, **16**, 701–708.
21 J. Sun, Y. Liu, J. M. Ritchie and X. Luo, *Proc. Inst. Mech. Eng., Part E*, 2015, **229**, 290–298.
22 W. W. Yu, E. Chang, J. C. Falkner, J. Zhang, A. M. Ali-Somali, C. M. Sayes, J. Jones, R. Drezek and V. L. Colvin, *J. Am. Chem. Soc.*, 2007, **129**, 2871–2879.
23 W. W. Yu, L. Qu, W. Guo and X. Peng, *Chem. Mater.*, 2003, **15**, 2854–2860.
24 W. W. Yu, L. Qu, W. Guo and X. Peng, *Chem. Mater.*, 2004, **16**, 560.
25 G. Baffou, J. Polleux, H. Rigneault and S. Monneret, *J. Phys. Chem. C*, 2014, **118**, 4890–4898.
26 X. M. Liu, L. Bao, M. Dipalo, F. De Angelis and X. H. Zhang, *Sci. Rep.*, 2015, **5**, 18515.
27 G. Baffou, R. Quidant and F. J. G. de Abajo, *ACS Nano*, 2010, **4**, 709–716.
28 C. Pang, Z. Zhao, J. G. Zhang, L. Shi, L. D. Du, Z. Fang and Y. H. Liu, *4th IEEE International Conference on Nano/Micro Engineered and Molecular Systems, Vols 1 and 2*, 2009, pp. 270–273, DOI: 10.1109/Nems.2009.5068575.
29 X. Y. Wang, J. Y. Zhang, A. Nazzal and M. Xiao, *Appl. Phys. Lett.*, 2003, **83**, 162–164.

30 G. V. Shcherbatyuk, R. H. Inman and S. Ghosh, *J. Appl. Phys.*, 2011, **110**, 053518.
31 A. Kongkanand, K. Tvrdy, K. Takechi, M. Kuno and P. V. Kamat, *J. Am. Chem. Soc.*, 2008, **130**, 4007–4015.
32 C. H. Wang, T. T. Chen, Y. F. Chen, M. L. Ho, C. W. Lai and P. T. Chou, *Nanotechnology*, 2008, **19**, 115702.
33 K. Tvrdy, P. A. Frantsuzov and P. V. Kamat, *Proc. Natl. Acad. Sci. U. S. A.*, 2011, **108**, 29–34.
34 T. B. Hoang, G. M. Akselrod, C. Argyropoulos, J. N. Huang, D. R. Smith and M. H. Mikkelsen, *Nat. Commun.*, 2015, **6**, 7788.
35 L. Zhang, C. Chen, W. Li, G. Gao, P. Gong and L. Cai, *ACS Appl. Mater. Interfaces*, 2016, **8**, 13187–13191.